THE JOURNAL OF PHYSICAL CHEMISTRY A

Article

pubs.acs.org/JPCA

Dissociative Photoionization of Dimethyl Carbonate: The More It Is Cut, the Bigger the Fragment Ion

Xiangkun Wu,[†] Xiaoguo Zhou,*[,†] Patrick Hemberger,[‡] and Andras Bodi*[,‡]

[†]Hefei National Laboratory for Physical Sciences at the Microscale and Department of Chemical Physics, National Synchrotron Radiation Laboratory, University of Science and Technology of China, Hefei 230026, China

[‡]Laboratory for Femtochemistry and Synchrotron Radiation, Paul Scherrer Institute, 5232 Villigen, Switzerland

ABSTRACT: The dissociation of internal energy selected dimethyl carbonate (DMC) cations was studied by imaging photoelectron photoion coincidence spectroscopy (iPEPICO) in the 10.3−12.5 eV photon energy range. Vibrational fine structure is observed in the ground state band of the threshold photoelectron spectrum up to the dissociation threshold, and Franck−Condon simulations identify the O—C—O bend mode, in particular in combination with the C═O stretch mode, to be active. The DMC ionization energy was determined to be 10.47 ± 0.01 eV. The first dissociative photoionization product, CH_2OH^+, dominates the breakdown diagram from 11.0 to 11.8 eV and is also the lightest fragment ion at m/z = 31. Statistical modeling of the PEPICO data yields a 0 K appearance energy of E_0 = 11.14 ± 0.01 eV. At higher photon energies, parallel dissociation channels are observed, leading to the daughter ions $C_2H_6O_2^+$, probably $OHCH_2CH_2OH^+$ (m/z = 62, E_0 = 11.16 eV), CH_3CHOH^+ (m/z = 45, E_0 = 11.46 eV), and CH_3OCO^+ (m/z = 59, E_0 = 11.47 eV). The m/z = 62 ethylene glycol ion may lose a CHO fragment and yield $CH_3OH_2^+$ (m/z = 33) in a sequential dissociation at E_0 = 11.54 ± 0.03 eV. Reaction path calculations explain the observed dissociation processes, except for the formation of the ethylene glycol cation. Composite method calculations of isodesmic and isomerization reaction energies are used to obtain the enthalpy of formation of dimethyl carbonate at $\Delta_f H^\circ_{0K}(DMC(g))$ = −548.3 ± 1.5 kJ mol^{-1}. This puts the heat of formation of the cation at $\Delta_f H^\circ_{0K}(DMC^+(g))$ = 461.9 ± 1.8 kJ mol^{-1}.

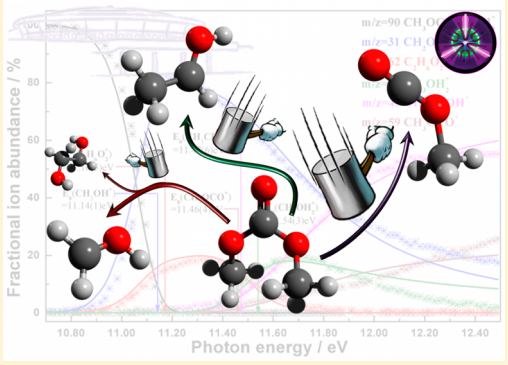

1. INTRODUCTION

Dimethyl carbonate (DMC) is the methyl ester of carbonic acid and is known to be a weak, but environmentally friendly methylating agent.[1] It can be used instead of dimethyl sulfate and methyl halides in methylation reactions.[2,3] DMC replaces phosgene as a methoxyl carbonylation agent in the formation of polycarbonates and carbamates. Thanks to its low toxicity and biodegradability, and recent advances in its synthesis in large quantities from methanol and carbon dioxide, it has been proposed not only as a green reagent but also as a green solvent,[4] and as an electrolyte in lithium ion batteries.[5] Because it is highly miscible with diesel fuels, it has potential as an oxygenated fuel blending agent promising cleaner combustion, thanks to its capability of reducing the concentration of soot precursor radicals.[6,7] It lowers the vapor pressure of the fuel, decreases carbon monoxide emissions, and does not increase NO_x emissions.[8,9]

DMC has also attracted interest because of its multifaceted conformational behavior, which motivated infrared and microwave spectroscopy as well as computational studies.[10−12] Lovas et al. reported the microwave spectrum of *cis*−*cis* dimethyl carbonate[13] and also calculated the relative energies of 13 isomers in the $C_3H_6O_3$ family at the MP2/6-311++G(d,p) level of theory. They found that only three isomers, lactic acid, 3-hydroxypropanoic acid, and hydroxymethyl acetate, are more stable than DMC, by 55, 53, and 33 kJ mol^{-1}, respectively.

Photoionization mass spectrometry (PI-MS) is a powerful technique to study combustion and pyrolysis processes individually and in model systems.[14−19] PI-MS can be combined with the kinetic energy analysis of the coincident photoelectron in photoelectron photoion coincidence spectroscopy[20] to identify reaction or pyrolysis decomposition product isomers selectively.[21,22] However, when an m/z peak is assigned in the mass spectrum, it is of constant concern whether the detected ion is a parent ion of a neutral reaction product or a fragment ion produced in a dissociative ionization process. Therefore, in pyrolysis or combustion studies using VUV photoionization, the dissociative ionization mechanism of the precursor has to be established in advance.[23,24] In addition, the dissociative ionization of DMC may provide insights into reaction mechanisms, as well as quantitative energetics data, such as ionization and activation energies and, should any of the dissociative ionization thresholds correspond to dissociation energies, even heats of formation.[25]

Received: January 17, 2017
Revised: March 4, 2017
Published: March 20, 2017

ACS Publications © 2017 American Chemical Society

DOI: 10.1021/acs.jpca.7b00544
J. Phys. Chem. A 2017, 121, 2748−2759

Highly oxygenated compounds often ionize dissociatively even at the ionization onset,[26] and it is advantageous to establish a photon energy window in which the parent ion is stable. Because the parent ion peak is observed in the electron ionization mass spectrum of DMC,[27] we are hopeful that such a window exists. Thus, the decay mechanism of energetic DMC^+ parent ions can be understood by using imaging photoelectron photoion coincidence (iPEPICO) spectroscopy. At the same time, a statistical model of the dissociative photoionization will enable us to predict DPI processes as a function of sample temperature, as well as facilitating data analysis at elevated temperatures.

The photoionization of DMC was studied in the 1970s by Meeks and McGlynn et al.[28,29] and Wittel et al.[30] by low-resolution photoelectron spectroscopy. They assigned the photoelectron bands on the basis of molecular orbital calculations and observed no vibrational fine structure. The overall DPI mechanism of DMC has not yet been studied. Appearance energies have been reported by electron ionization for m/z = 59 (11.5 or 12.2 eV)[31,32] and m/z = 60 (11.5 eV). The large difference in the former set of values does not justify the claimed 0.05−0.08 eV error bar, and the latter ion has not been observed in the experiments herein. Thus, it appears that some of these onsets have not stood the test of time.

The dissociative photoionization of DMC, $CH_3OC(=O)OCH_3$, can be related to that of other small esters, as discussed more recently by Wang et al.[33] Generally, they found that dissociation channels often arise from complex isomerization processes in competition with direct bond breaking in the parent ion. This was also observed by Suh et al. for the methyl glycolate cation, $HOCH_2C(=O)OCH_3^+$,[34] in which HCO loss takes place by double hydrogen transfer by the H-bonded intermediate $H_2C{=}O{\cdots}H{\cdots}O{=}COCH_3^+$. Methyl glycolate cations may also rearrange to DMC^+, which Suh et al. identified as the driving force for CH_2OH^+ (m/z = 31) formation. Methyl-β-hydroxypyruvate $[CH_3OC(=O)C(=O)CH_2OH]$ and dimethyl oxalate $[CH_3OC(=O)C(=O)OCH_3]$ are also similar compounds to DMC. In dissociative photoionization, both may lose CO to form a $C_3H_6O_3^+$ ion, isomer with DMC^+.[35,36] However, m/z = 60 and 61, i.e., $HOCOCH_3^+$ and $HOC(H)OCH_3^+$ have been identified as the main collision-induced dissociation and dissociative photoionization products of these $C_3H_6O_3^+$ isomers. Although the involvement of the DMC^+ was invoked to explain isotope mixing in the fragmentation of the above-mentioned ions, m/z = 60 and 61 ions are not observed as major products in the DPI of DMC (vide infra). This leads us to believe that we can rule out the isomerization of the DMC cation to the above-mentioned H-bonded intermediate or methyl glyconate, and the reverse process, i.e., the formation of DMC^+, is irreversible and quickly followed by dissociation. Thus, the fragmentation of DMC^+ takes place in a comparatively separated subspace of the $C_3H_6O_3^+$ potential energy surface compared with the isomers studied before in detail.

Trikoupis et al. studied another interesting dissociative ionization process of dimethyl oxalate, in which the molecular ion seemingly breaks in half, and does so 0.5 eV (50 kJ mol^{-1}) below the calculated barrier to $CH_3OC{=}O + CH_3OC{=}O^+$ formation.[37] Collision-induced dissociation experiments unveiled the true mechanism, in which CO_2 and CH_3 are released without the intermediacy of the less stable CH_3OCO radical. Because $CO_2 + CH_3$ is more stable separately than bound,[31,38] it is no surprise that 59 amu loss takes place in two steps. The intriguing aspect is that the intermediate, 15 or 44 amu loss cation has not been detected. In dimethyl oxalate, the proposed reaction energy curve involves a CO_2-loss intermediate $CH_3OCOCH_3^+$ potential energy well of at least 0.7 eV or almost 70 kJ mol^{-1}. The m/z = 54 intermediate could be stabilized by kinetic energy release or rovibrational excitation of the leaving CO_2 molecule but has not been observed experimentally. A bifurcated $CH_3 + CO_2$- or $CO_2 + CH_3$-loss reaction pathway was identified in the DPI of acetic acid anhydride $[CH_3C(=O)OC(=O)CH_3]$, in which the intermediate CO_2-loss acetone cation also sits in a 0.8 eV deep potential energy well and is only formed with 0.16 eV excess energy at the transition state.[25] However, the intermediate acetone cation as well as the minor methane-loss channel from the acetone cation[39] could be observed in very small amounts here. Generally, both in these dissociation mechanisms and in the water loss in adipic acid at the ionization onset,[26] the underlying theme is that isomerization reactions leading to a significantly more stable constitutional isomer are associated with low barriers on the cation potential energy surface in these oxygenated organic compounds. This opens up fragmentation channels, sometimes even sequential ones, at energies much lower than any of the bond energies in the parent ion. The dissociative ionization mechanism of DMC, in particular the production of the first and lightest fragment at m/z = 31, will also be shown to be best explained by sequential methyl radical and carbon dioxide loss with an unseen and short-lived intermediate.

We report imaging photoelectron photoionization coincidence (iPEPICO)[40] data on DMC taken at the VUV beamline of the Swiss Light Source, use quantum chemical calculations to establish the dissociation mechanism of the DMC^+ cation, and set up a statistical model to determine experimental 0 K appearance energies for the DPI channels. Plotting and analyzing the fractional threshold ionization parent and daughter ion abundances in the breakdown diagram has been shown to reveal directly complex dissociative photoionization mechanisms involving multiple isomerization steps.[41−43] We have determined accurate 0 K appearance energies for the main DPI channels leading to the fragments of m/z = 31, 62, 33, 45, and 59. The small abundance of m/z = 61 and 60 confirms that DMC^+ is unlikely to form the hydrogen bonded intermediate $H_2C{=}O{\cdots}H{\cdots}O{=}COCH_3^+$, known to be an important crossroads in the dissociation of other $C_3H_6O_3^+$ isomers. Furthermore, the threshold photoelectron spectrum shows vibrational fine structure at the ionization onset, which is modeled to confirm the adiabatic ionization energy of DMC. Composite method calculations are used to derive the heat of formation of DMC, which anchors the derived appearance energies to the thermochemical heat of formation scale.

2. METHODS

2.1. Experimental Approach. The photoionization experiments were performed at the VUV beamline of the Swiss Light Source, Paul Scherrer Institute, using the Imaging Photoelectron Photoion Coincidence (iPEPICO) endstation. A detailed description of the beamline and the iPEPICO experiment can be found elsewhere,[40,44] and only a brief overview is given here. Bending magnet synchrotron radiation is collimated, dispersed by a grazing incidence monochromator using a 600 lines/mm laminar grating, and focused into a differentially pumped gas filter to suppress higher-order radiation. The gas filter is filled with 10 mbar of a neon,

DOI: 10.1021/acs.jpca.7b00544
J. Phys. Chem. A 2017, 121, 2748−2759

argon, and krypton mixture, effectively extinguishing radiation above 14 eV in a 10 cm long absorption chamber. The high-harmonic free, monochromatic VUV radiation enters the ionization chamber of the iPEPICO endstation and ionizes the sample in a 4×2 mm^2 cross section interaction region. The photon energy is calibrated using argon autoionization lines, recorded in first and second order of the grating, and the photon energy resolution is 3−4 meV.

Dimethyl carbonate was purchased from Sigma−Aldrich and used without further purification. It was kept at room temperature in a sample holder and seeded into the ionization chamber through a needle valve and a 6 mm outer diameter Teflon tube. The typical pressure in the experimental chamber was 3×10^{-6} mbar during measurement. In the interaction region, the VUV light crosses the effusive sample beam and the resulting photoelectrons and photoions are extracted in opposite directions by a constant, 120 V cm^{-1}, electric field. The electrons are then velocity map imaged onto a position sensitive Roentdek DLD40 delay-line detector with a kinetic energy resolution better than 1 meV at threshold. As their time-of-flight (TOF) is negligible, electron hit times can be used as the start signal for the ion TOF analysis. The ions are extracted in a 5 cm long first extraction region and then undergo further acceleration to ensure space focusing conditions at a Jordan TOF C-726 microchannel plate detector at the end of a 55 cm long field-free drift region. The arrival times of the photoelectrons are correlated with that of the photoions to obtain the ion TOF distributions. The ion hits as stop signals and arrival times are recorded using a triggerless multiple-start/multiple-stop data acquisition scheme.[45]

Threshold electrons are imaged onto a central spot on the detector together with kinetic energy electrons with negligible off-axis momentum component. The latter make up the hot electron contamination, which can be approximated on the basis of a small ring around the center spot and subtracted from the center signal as proposed by Sztáray and Baer.[46] The threshold photoelectron signal is plotted as a function of the photon energy in the threshold photoelectron spectrum (TPES). The coincident threshold photoionization mass spectra are two-dimensional; i.e., they correspond to the ion signal as a function of TOF and photon energy. The fractional parent and fragment ion abundances are plotted in the breakdown diagram as a function of photon energy, which shows the open fragmentation channels and their branching ratio as a function of photon energy, and is independent of the photon flux or the sample pressure and only depends on the temperature and, in the case of a slow dissociation, the residence time of the parent ion in the extraction region. The use of a relatively low extraction field leads to ion residence times in the acceleration region of several microseconds and yields a quasi-exponential daughter ion peak shape in metastable dissociations. It is indicative of the dissociation rate constant in the kinetic time window, in our case 10^3 s$^{-1} < k < 10^7$ s^{-1}.[20] In a fast dissociation, the breakdown diagram of the parent ion is determined by its internal energy distribution, i.e., the experimental temperature. The 0 K appearance energy corresponds to the photon energy at which even the neutrals in the rovibrational ground state gain enough internal energy to dissociate, and the parent ion disappears from the breakdown diagram. If the dissociation is slow, some excess energy, called the kinetic shift, is needed for the parent ion to dissociate on the experimental time scale. The dissociation rate curve is recorded and extrapolated to the onset using a statistical approach to determine the kinetic shift.

2.2. Quantum Chemical Calculations. Computed rotational constants and harmonic vibrational frequencies are used to calculate the thermal energy distribution of the sample, and as input for the density and number of states calculations to obtain the *ab initio* rate curves as the starting point of the statistical model fit. The product energy distribution, i.e., the partitioning of the excess energy between the fragment ion, the neutral, and the newly formed translational degrees of freedom, is also determined on the basis of rovibrational densities of states of the fragments. This is needed to calculate the breakdown curves corresponding to the sequential dissociation process, when the fragment ion dissociates further, and its internal energy distribution is shifted and broadened by the product energy distribution. Furthermore, the potential energy surface is explored to establish the reaction coordinates corresponding to the observed fragmentation channels. Although the rate curves are fitted to the experimental data, harmonic frequencies evaluated at the correct stationary points along the reaction coordinate also make the statistical model more trustworthy.

The reaction potential energy curves were calculated by density functional theory at the B3LYP/6-311++G(d,p) level in constrained optimizations. Transition states were also located using the Synchronous Transit-Guided Quasi-Newton method.[47] Normal mode analysis was carried out to evaluate vibrational frequencies, zero-point energies, and to confirm minima and transition state geometries. The total energies were further refined at the stationary points using Gaussian-4 (G4) theory.[48]

When appearance energies correspond to dissociative photoionization energies, thermochemical values, such as enthalpies of formation or protonation affinities can be derived on the basis of literature thermochemical data and the onset energies by the ion cycle.[49] As will be shown later, the dissociative photoionization mechanism of DMC is governed by high-lying transition states, which precludes this approach. However, to reference the measured appearance energies to the standard thermochemical scale of enthalpies of formation, we calculated isodesmic and isomerization reaction energies to confirm the DMC heat of formation using the G4, CBS-APNO, and W1U methods.[50,51]

We have also observed vibrational fine structure along the rising edge of the ground state band in the photoelectron spectrum. Franck−Condon factors and room temperature peak intensities were calculated using ezSpectrum 3.0[52] based on the B3LYP/6-311++G(d,p) Hessian obtained with Q-Chem 4.3.[53] The ωB97X-D/cc-pVTZ Hessian was also evaluated, and the computed vibrational structure agreed well with the B3LYP result. The electronic excited states of the cation were also calculated using Q-Chem at the EOM-IP-CCSD/cc-pVQZ level of theory. The Gaussian 09 program was used in all other calculations.[54]

2.3. Statistical Modeling. The threshold photoionization TOF mass spectra reveal the fragment ions in the energetically and kinetically allowed dissociation channels, as well as the dissociation rate constant in the 10^3 s$^{-1} < k(E) < 10^7$ s^{-1} range. A statistical model is constructed on the basis of the observed fragmentation channels and computed vibrational frequencies and rotational constants, and appearance energies are fitted to reproduce the fractional ion abundances, relative dissociation rate constants as observed in the breakdown diagram as

DOI: 10.1021/acs.jpca.7b00544
J. Phys. Chem. A 2017, 121, 2748−2759

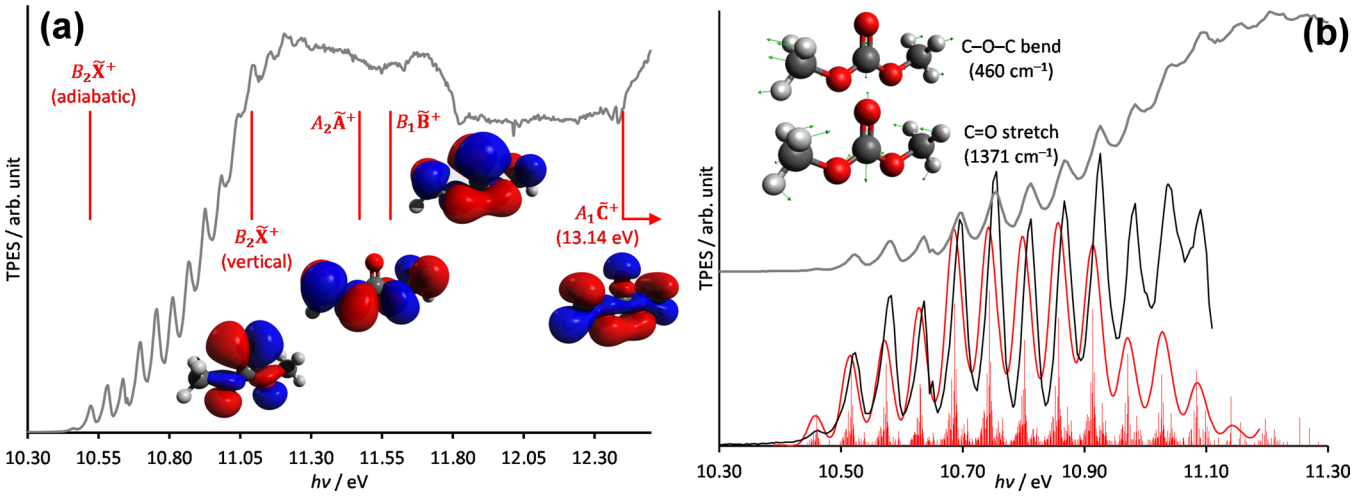

Figure 1. Threshold photoelectron spectrum of dimethyl carbonate from 10.30 to 12.50 eV. The EOM-IP-CCSD vertical ionization energies are shown together with the molecular orbital dominating the transition. The computed adiabatic ionization energy is also shown in (a). After a cubic baseline is subtracted, the ground state TPES (shown in black) is compared with the Franck−Condon model by convoluting the transitions (red sticks) with a 12 meV FWHM Gaussian function. By fitting the 0−0 transition, an experimental ionization energy of 10.47 eV is reported (see text). The ionic vibrational modes determining the vibrational fine structure, namely, the O—C—O bend and C═O stretching modes, are illustrated in (b), as well.

branching ratios and absolute rate constants, measured in the form of peak shapes in the mass spectrum. Our approach is described in detail by Sztáray et al.,[55] and only the most important aspects are mentioned here.

In threshold photoionization, the internal energy of the parent ion, available of dissociation, is established as the sum of the internal energy of the neutral and the photon energy, minus the adiabatic ionization energy. If the parent ion is metastable and there is a kinetic shift, the density of states of the parent ion and the number of states of the transition state are used to calculate the unimolecular dissociation rate constant according to the RRKM theory as[56−58]

$$k(E) = \frac{\sigma \cdot N^{\ddagger}(E - E_0)}{h \cdot \rho(E)} \quad (1)$$

where $N^{\ddagger}(E-E_0)$ is the number of states at the transition state at excess energy $E - E_0$ above the dissociation barrier or 0 K appearance energy E_0, $\rho(E)$ is the density of states of the dissociating ion, h is Planck's constant, and σ corresponds to the symmetry of the reaction coordinate. The statistical model is fitted to reproduce the breakdown diagram and the time-of-flight distributions simultaneously. To do so, the appearance energy is changed, and the transitional mode vibrational frequencies, i.e., the ones turning to barrierless rotations and translations during the dissociation, are scaled by an adjustable factor to fit the rate curves.

When fragment ions dissociate further, the model partitions the excess energy among the intermediate ion, the leaving neutral and the newly created transitional degrees of freedom according to statistical theory,[59] and the internal energy of the intermediate is then available in the subsequent fragmentation process.

3. RESULTS AND DISCUSSION

3.1. Threshold Photoelectron Spectrum. The TPES of DMC was recorded in 4.5 meV steps and 2 min integration time in the 10.3−12.5 eV photon energy range. The spectrum, shown in Figure 1a, differs from the He photoelectron spectrum by McGlynn and Meeks,[29] because the intensity does not drop significantly between 11.9 and 12.3 eV. Close above the ionization energy, there is a high density of Rydberg states. Excitation to this manifold may lead to threshold autoionization, which contributes to the filling up of the threshold photoelectron spectrum even in Franck−Condon gaps.[60,61] This is a general phenomenon, which indeed makes threshold photoelectron photoion coincidence quite appealing, because it guarantees the production of internal energy selected parent ions at all energies,[62] except in very broad Franck−Condon gaps.[63] However, if autoionization is the main reason for the elevated baseline in the TPES between 11.8 and 12.3 eV, it would have to be an uncharacteristically strong process. To clarify this, we calculated the vertical ionization energies of DMC at the EOM-IP-CCSD/cc-pVQZ level of theory at the neutral geometry. The vertical ionization energies to the $\tilde{X}^2B_2$, $\tilde{A}^2A_2$, $\tilde{B}^2B_1$, $\tilde{C}^2A_1$, and $\tilde{D}^2B_2$ states were found to be 11.09, 11.47, 11.58, 13.14, and 13.76 eV, respectively, with the symmetry labels given with *yz* as the principal plane of the molecule (see also the corresponding molecular orbitals in Figure 1a). No additional state was found close to 12 eV, and the energy of the first quartet cation state is calculated to be 15.23 eV (G4 value), which speaks for enhanced autoionization as the sole source for the threshold electron signal around 12 eV.

The adiabatic ionization energy of DMC has been calculated to be 10.52, 10.48, 10.54, and 10.56 eV using the EOM-IP-CCSD/cc-pVQZ with W1 zero-point energy, G4, CBS-APNO, and W1U methods. Unlike previous photoelectron spectra, our TPES offers a sufficient resolution to resolve vibrational fine structure on the rising edge of the ground state band, as shown in Figure 1b. The unstructured contributions of the higher-lying states and the autoionization signal was approximated by a cubic baseline, which was subtracted from the TPES. The resulting black trace can be compared with the room temperature Franck−Condon simulation, convoluted with a 12 meV full width at half-maximum Gaussian curve. Due to the strong autoionization backdrop to the vibrational progression, the computed vibrational line intensities show some deviations

DOI: 10.1021/acs.jpca.7b00544
J. Phys. Chem. A 2017, 121, 2748−2759

when compared with the experiment, but this does not affect the assignment significantly. Furthermore, Franck−Condon calculations show that the first vibrational band, least affected by autoionization, should be observable, and it is based on this that we assign the adiabatic ionization energy. We can, thus, establish the position of the 0 ← 0 transition as 10.46 eV, which, when taking into account the Stark shift at a constant field of 120 V cm^{-1},[64] corresponds to a DMC ionization energy of 10.47 eV. The observed vibrational transitions are dominated by excitation of O—C—O bend in the cation at 460 cm^{-1}. The C═O stretching mode at 1371 cm^{-1} is also quite active, particularly in combination with the O—C—O bending mode. In the ion, the C═O bond length increases to 1.30 Å from 1.20 Å in the neutral, and the O—C—O bond angle increases to 118.7° from 107.9° in the neutral, whereas the C—O bond length decreases to 1.27 Å from 1.34 Å. These two normal modes (see also in Figure 1b) explain most of the vibrational fine structure observed in the ion.

The vibrational structure vanishes as we move to the energy range of the first excited $\tilde{A}^2A_2$ ionic state. This coincides with the onset of dissociative photoionization, but the main reason for the broadening of the spectral features is expected to be fast internal conversion to the ground electronic state, and the resulting short lifetime of the initial ion or Rydberg states. On this basis, and on the basis of the faithful reproduction of the breakdown diagram with a statistical model (see below), the dissociative photoionization of DMC passes the "duck test" of statistical dissociation. This is also supported by the absence of fast, impulsive processes[65] as well as breakdown curves that correlate with TPES features.[66]

3.2. Dissociative Photoionization Mass Spectra. Threshold photoionization mass spectra were recorded in the 10.3−12.5 eV photon energy range. Six representative TOF distributions are shown in Figure 2, with peaks seen at m/z =

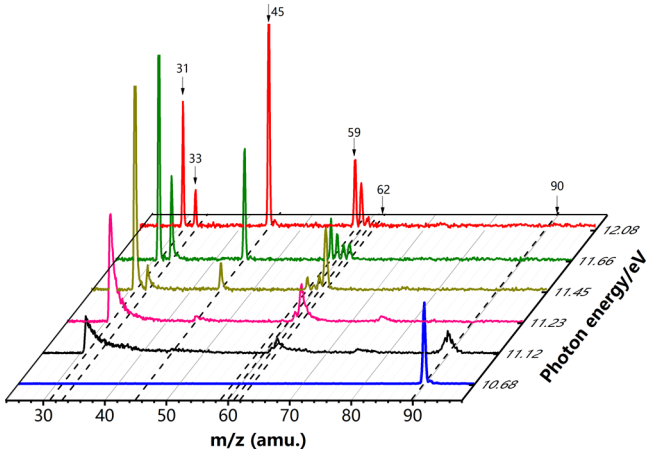

Figure 2. Threshold photoionization mass spectra shown at a few representative photon energies.

90, 75, 62, 61, 60, 59, 45, 33, and 31. Among these, m/z = 61 is only present in small amounts, and its abundance follows that of m/z = 62, whereas the abundance of m/z = 60 is smaller than and evolves similarly to that of m/z = 59. The fractional ion abundance of the main ions is plotted as a function of photon energy in the breakdown diagram in Figure 3.

The first dissociation channel of the m/z = 90 DMC parent ion leads to the m/z = 31 ion, which dominates the threshold ionization mass spectrum from 11.0 to 11.8 eV. The TOF peak

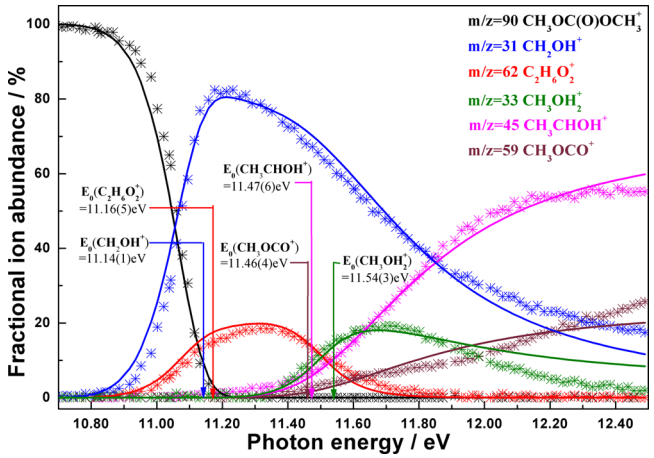

Figure 3. Breakdown diagram of dimethyl carbonate between 10.70 and 12.50 eV. Crosses correspond to measured fractional abundances and continuous lines show the best-fit model, based on which the appearance energies have been determined.

of m/z = 31 is asymmetric at its onset and becomes symmetric as the photon energy is increased, indicative of a metastable dissociation and a low rate constant at the barrier. The same applies to m/z = 62, the production of which competes with the m/z = 31 channel. The potential energy well of the DMC cation is relatively shallow, it is only bound by less than 1 eV. The dissociation rate at threshold is inversely proportional to the low density of states of the parent ion, and proportional to the transition state number of states, which consequently must be small for the parent ion to be metastable. This suggests a reverse barrier to dissociation, with an associated, tight transition state along the reaction coordinate, and makes it unlikely that the m/z = 31 ion is the result of C−O bond rupture yielding CH_3O^+, a process also ruled out by the G4-calculated onset, which is too high at 12.60 eV. Therefore, the CH_2OH^+ isomer ion must be the fragmentation product. There are two feasible pathways to yield CH_2OH^+ ion in the present experiment. The corresponding neutral fragments are CO_2 + CH_3 or CH_3OCO, and the dissociation limits are 10.58 and 11.54 eV, respectively. In the TOF distributions recorded at 11.115 eV, the parent ion peak at m/z = 90 is evidently broadened symmetrically in Figure 2. The symmetric broadening is the result of significant kinetic energy release (KER) upon dissociation: when a daughter ion is formed in the drift region of the mass spectrometer, it continues to fly toward the detector with the same average speed of the parent, but its velocity distribution may be broadened because of KER.[66] Therefore, the breakdown diagram indicates a large reverse barrier associated with large kinetic energy release in the first dissociation step, which, together with the *ab initio* energetics, makes it likely that this channel yields the most stable CH_2OH^+ + CO_2 + CH_3 products. This broadening may also hide a minor H-loss channel. However, we can rule such out, because lowest energy direct H-loss channel has a computed onset energy of 11.65 eV.

The fragment ion at m/z = 62 rises parallel to the major m/z = 31 channel and levels off at a maximum fractional abundance of 20% before disappearing from the breakdown diagram at 11.8 eV. As the m/z = 62 signal vanishes, the m/z = 33 rises, which is consistent with CHO (29 amu) loss from the m/z = 62 intermediate, yielding $CH_3OH_2^+$. Because of energetics, this rules out ethylene loss in the first step and implicates CO as the

DOI: 10.1021/acs.jpca.7b00544
J. Phys. Chem. A 2017, 121, 2748−2759

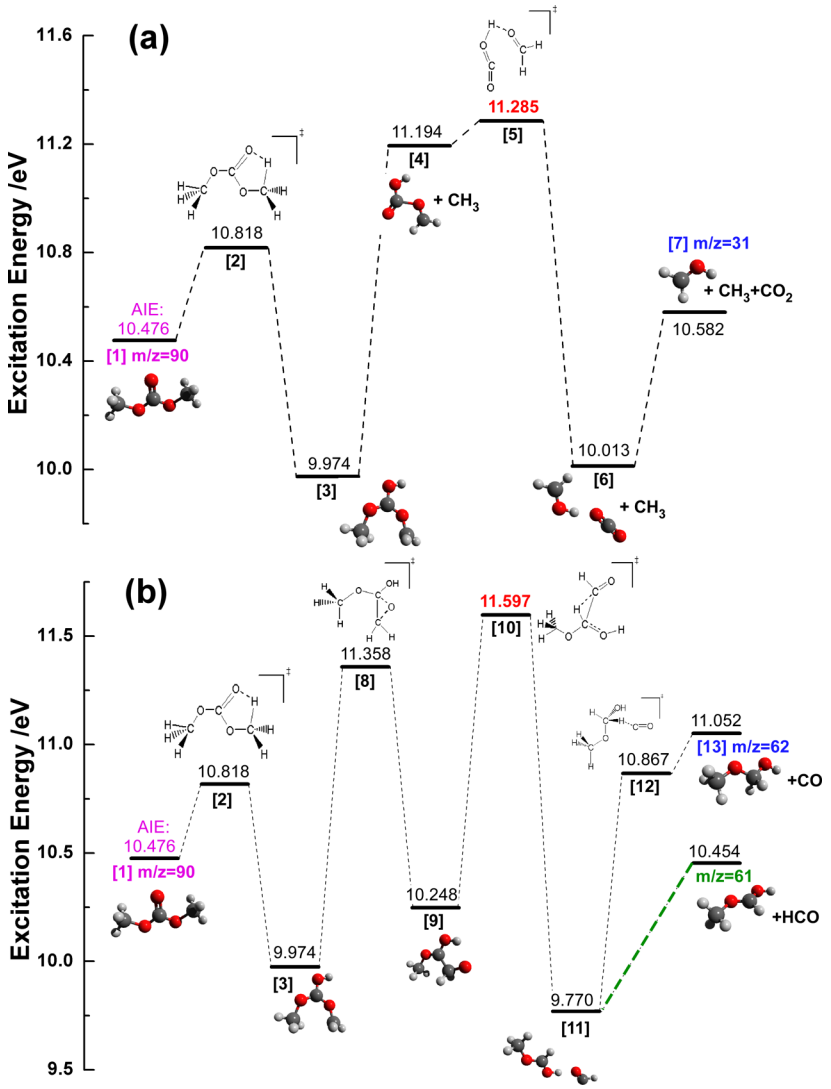

Figure 4. Computed fragmentation paths of the dimethyl carbonate cation to produce the m/z = 31 (a) and m/z = 62 (b) ion, relative to the neutral molecule. Minimum and transition state energies have been evaluated using the G4 composite method.

leaving neutral in the loss of 28 amu from DMC^+. This must involve H-transfer isomerization step(s) along the reaction coordinate. A small m/z = 61 ion peak is also observable in the TOF distributions, and as its abundance seems to mirror that of the m/z = 62 channel, it probably shares the rate determining transition state with the m/z = 62 channel. In contrast with previous studies on $C_3H_6O_3$ isomers, notably methyl glycolate,[34,36] in which the $CH_2{=}O{\cdots}H{\cdots}O{=}COCH_3^+$ intermediate predominantly yields m/z = 61 fragment by HCO loss, m/z = 61 is a small channel here, and this intermediate should play a limited role in the DPI of DMC. This leaves us with three likely potential m/z = 62 fragment ions, $CH_3OCH_2OH^+$, $HOCH_2CH_2OH^+$, and $CH_3OOCH_3^+$, among which ethylene glycol yields most $CH_3OH_2^+$ when fragmenting.[27]

Above 11.3 eV photon energy, fragmentation channels open up to m/z = 45 and 59, as well. Both stoichiometric reasons and the slope of the corresponding breakdown curves speak for a parallel mechanism from the DMC^+ cation: these two fragment ions correspond to the loss of 45 (CHO_2 or C_2H_5O) and 31 amu (CH_3O). Furthermore, there is a bend in the m/z = 59 breakdown curve at a photon energy of 11.9 eV, which suggests that two different mechanisms may be at play.

The m/z = 45 channel corresponds to breaking the parent ion in half. Because the calculated dissociation energy to $C_2H_4OH^+$ or $CH_2OCH_3^+$ with H + CO_2 as neutral fragments is more than 1 eV lower than that to $OCOH^+$ + CH_3CHOH, we conclude that this channel likely corresponds to $C_2H_5O^+$ + H + CO_2 production. As for m/z = 59, the G4-calculated onset energy for the direct loss of CH_3O by C−O bond breaking lies at 11.79 eV, which suggests that this process contributes to the second part of the breakdown curve, above 11.9 eV. At lower energies, the more stable CH_2OH is the likely leaving neutral fragment, with a dissociative photoionization energy of 11.42 eV, corresponding to the formation of CH_3CHOH^+. Protonated glyoxal, $HOHCCHO^+$, another $C_2H_5O^+$ isomer, is less stable than CH_3OCO^+. The m/z = 60 ion has also been observed in trace amounts, with its abundance mirroring that of m/z = 59, which suggests that the two channels share the rate determining transition state.

Besides the fragment ions described above, we have also observed a minor peak at m/z = 75 in the low photon energy range. This fragment, corresponding to the loss of a methyl

DOI: 10.1021/acs.jpca.7b00544
J. Phys. Chem. A 2017, 121, 2748−2759

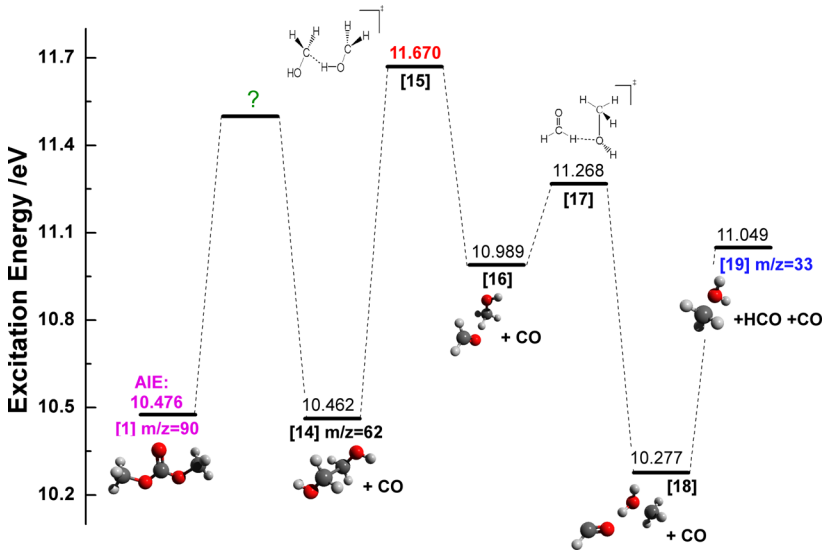

Figure 5. m/z = 33 production pathway from the ethylene glycol cation [**14**] (m/z = 62), relative to the neutral DMC molecule. Minimum and transition state energies have been evaluated using the G4 composite method.

radical, appears at the same photon energy as the m/z = 31 ion and disappears when the m/z = 31 peak becomes symmetric. The mechanism of 59 amu loss leading to the CH_2OH^+ ion therefore appears to be a two-step process, with a methyl group first leaving, prior to CO_2 loss. This is similar to the CO_2 + CH_3-loss mechanism proposed by Trikoupis et al. for the oxalate ion,[37] only that the methyl radical seems to leave first from DMC^+. In the acetic acid anhydride cation,[25] both CH_3 + CO_2 and CO_2 + CH_3 processes could be observed along a shared reaction path bifurcated past the isomerization transition state, although the CO_2-loss intermediate, the acetone cation, was only present in trace amounts. Consequently, such concerted methyl- and carbon dioxide-loss fragmentation channels appear to be quite common in highly oxygenated organic cations.

3.3. Potential Energy Surface. On the basis of the breakdown diagram, the dissociative photoionization of DMC is governed by isomerization transition states that form the leaving groups by, e.g., hydrogen transfer. The weakest direct bond breaking channel corresponds to H loss at 11.65 eV, of which we see no experimental evidence. At 11.79 eV, C−O bond rupture may yield the OCH_3 neutral fragment, which process may contribute to the m/z = 59 signal above 11.9 eV photon energy. When cationic dissociations take place along a purely attractive potential energy curve, the product energies will govern the process. However, because of isomerization transition states in DMC, the dissociative photoionization energies are not accessible experimentally by iPEPICO, only the activation energies and the dynamics are determined by the tight isomerization transition states. We carried out numerous constrained optimizations scanning bond lengths and angles, as well as reaction path optimizations to locate these rate determining transition states and unveil the following fragmentation channels of DMC ion: (1) production of m/z = 31 ion, by methyl and carbon dioxide loss, (2) CO loss yielding $C_2H_6O_2^+$ at m/z = 62, (3) sequential HCO loss from m/z = 62 to yield $CH_3OH_2^+$, (4) the formation of $C_2H_5O^+$ at m/z = 45 by carbon dioxide and hydrogen atom loss, (5) isomerization controlled and direct C−O bond dissociation to yield the m/z = 59 fragment ion. The transition state vibrational frequencies are also used as a starting point for the number of states calculation in the statistical model. Contrary to previous DPI studies on complex mechanisms, for instance on an Arduengo-type carbene,[41] quinoline,[67] or adipic acid,[26] our approach has not delivered a fully consistent set of reaction paths, and, as will be discussed later, suitable transition states could not be located to m/z = 62 formation. Constrained optimizations are bound to fail if the reaction coordinate changes in character as the reaction proceeds, e.g., if a torsional motion precedes significant changes in bond lengths. Redundant internal coordinate based reaction path calculations also assume a steady change in internal coordinates and may not locate the transition state if it lies significantly off the diagonal connecting the product with the reactant. We believe that the missing transition states could only be located by a more systematic and automatic exploration of the potential energy surface, which also underlines the need for methods development.[68−70]

Figures 4−6 display the most important stationary points, minima, and transition states involved in the dissociative photoionization process of DMC. As shown in Figure 4a, the ground state ion geometry [**1**] is calculated at 10.48 eV with respect to the neutral DMC. A hydrogen atom is transferred to the (C═)O by a five-membered ring transition state [**2**]. The DMC isomer $CH_3OC(OH)CH_2^+$ ion [**3**] is 0.50 eV more stable than the parent ion. The CH_3−OC bond can be broken in a fast reaction at 11.194 eV to yield the m/z = 75 methyl-loss product CH_2OCOOH^+ [**4**]. This ion is barely bound and can undergo H-transfer to $H_2COH\cdots OCO$ over transition state [**5**] at 11.29 eV. The hydrogen bond is broken and CO_2 is released in intermediate [**6**] at 10.58 eV, which yields the main CH_2OH^+ fragment ion at m/z = 31 [**7**].

Based on their parallel rise, the m/z = 62 and 31 channels appear to be governed at least in part by the same rate-determining step. A C−C bond can indeed be formed in the isomer DMC ion [**3**] over a three-membered COC transition state [**8**] at 11.36 eV. The resulting $CH_3OC(OH)CH_2O^+$ intermediate [**9**] at 10.25 eV can undergo H-transfer from the CH_2 group to the central C atom over transition state [**10**] at an energy of 11.60 eV. The product of this H-transfer is the

DOI: 10.1021/acs.jpca.7b00544
J. Phys. Chem. A 2017, 121, 2748−2759

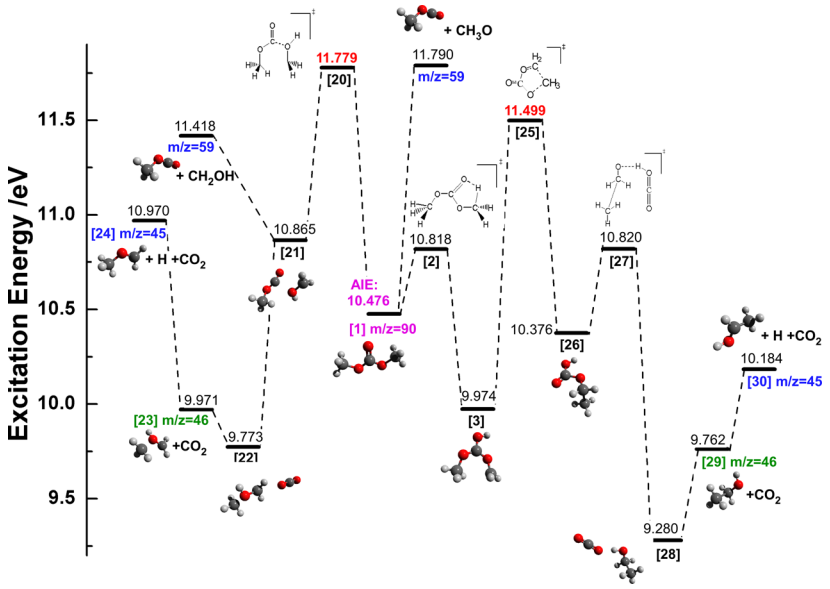

Figure 6. Fragmentation paths of the dimethyl carbonate cation to produce the m/z = 45 and m/z = 59 ions, relative to the neutral molecule. Minimum and transition state energies have been evaluated using the G4 composite method.

very stable $CH_3OCHOH\cdots OCH^+$ ion at 9.77 eV [**11**], which rearranges by H back-transfer from OCH to CH over transition state **12** at 10.87 eV and loses CO to yield the m/z = 62 ion, $CH_3OCH_2OH^+$ [**13**]. The overall fragmentation process is displayed in Figure 4b.

However, this mechanism has several shortcomings. First, the H-bond in $CH_3OCHOH\cdots OCH^+$ [**11**] is easiest to break and should predominantly yield m/z = 61 over a loose transition state in a fast dissociation already at 10.45 eV. Even more importantly, the transition state yielding m/z = 33, $CH_3OH_2^+$ from the expected m/z = 62 ion, $CH_3OCH_2OH^+$ [**13**], lies at 12.41 eV (not shown in Figure 4), whereas water loss from $CH_3OCH_2OH^+$ [**13**] to form the unobserved m/z = 44 ion appears to take place more readily at 11.55 eV. Therefore, the observed m/z = 62 ion looks unlike $CH_3OCH_2OH^+$ [**13**] and is in fact most likely to be the ethylene glycol cation, $HOCH_2CH_2OH^+$, which is known to form $CH_3OH_2^+$ dominantly when dissociating at low energies,[71] and for which we found an H-transfer transition state to $CH_3OH_2^+$ production at 11.67 eV. However, despite numerous attempts, we could not find an energetically feasible pathway to the ethylene glycol cation itself. As the experiment suggests, the unknown barrier height should be lower than 11.6 eV.

As mentioned above, the fractional ion abundance of m/z = 33 rises as the m/z = 62 signal decreases. Thus, the fragmentation channel is thought to be the HCO (29 amu) loss from the m/z = 62 intermediate. Once the m/z = 62 ethylene glycol cation [**14**] is produced, an isomer ion of $HCO\cdots H_2O\cdots CH_3^+$ [**18**] can be formed via a two-step hydrogen-transfer process, as displayed in Figure 5. The m/z = 33 $CH_3OH_2^+$ [**19**] is directly yielded by a sequential HCO loss from the complex ion [**18**]. The overall process is very similar to that in ref 71. The rate-determining barrier height is 11.67 eV, which agrees with the present experimental conclusion.

The m/z = 45 channel represents the parent ion losing half of its mass, and because of the ionization energy differences, the charge is likely to be carried off by the $C_2H_5O^+$ species. HCO_2 is higher in energy than H + CO_2; therefore, this process is also proposed to take place in two steps, similar to the CH_3 + CO_2 loss yielding m/z = 31. We have found a path over a H-transfer transition state [**20**] to the vicinal oxygen atom at 11.78 eV, and subsequently, the $OCO\cdots CH_2O(H)CH_3^+$ species [**22**] at 9.77 eV is yielded via a methyl transfer to the same oxygen from the $CH_3OC(O)O(H)CH_2^+$ [**21**]. Carbon dioxide leaves at already 9.97 eV, leaving behind a hot $CH_3O(H)CH_2^+$ ion at m/z = 46 [**23**] with potentially more than 1.5 eV excess energy. Afterward,$CH_3OCH_2^+$ [**24**] (m/z = 46) can be formed at an energy of 10.97 eV.

Alternatively, the CH_3 group in [**3**] may attack the CH_2 group to form $CH_3CH_2OC(=O)OH^+$ [**26**], i.e., the ethyl ester of carboxylic acid, at 10.38 eV over a transition state [**25**] at 11.50 eV. After a further hydrogen atom transfer over a 10.82 eV barrier, $CH_3CH_2OH^+\cdots OCO$ [**28**] is formed at 9.28 eV, which readily loses carbon dioxide at 9.76 eV to yield the ethanol cation. At this point, the system has 1.74 eV excess energy, 0.42 eV of which suffices to form the m/z = 45 ion $C_2H_4OH^+$ [**30**] at 10.18 eV.[72] Because the overall barrier to $CH_3CH_2OH^+$ formation is 0.28 eV lower than to $CH_3OHCH_2^+$ formation, the CH_3CHOH^+ isomer [**30**] may be the dominant m/z = 45 product in the mass spectra. Both pathways to yield the m/z = 45 ions are shown in Figure 6. Both m/z = 46 isomers could survive in the rare cases when most excess energy is carried away by CO_2. However, the m/z = 46 abundance is so small throughout the photon energy range that it is obscured by the 2.2% ^{13}C peak of m/z = 45.

This pathway also leads to the global cationic minimum among the isomers we explored. An H-transfer in the carboxylic acid ethyl ester cation [**26**] yields $CH_2CH_2OC(OH)_2^+$ at an energy of 9.05 eV, relative to the neutral DMC. Although this species is energetically accessible and is a prime candidate for ethylene glycol cation formation, it is instead more likely to lose an ethylene cation to yield carboxylic acid, H_2CO_3, at an energy of 10.71 eV. In the absence of an m/z = 28 signal, we can state that even this process is outcompeted by CO_2 loss yielding the ethanol cation and, eventually, the m/z = 45 fragment ion.

As mentioned earlier, two dissociation channels may yield the CH_3OCO^+ fragment ion at m/z = 59, depending on

DOI: 10.1021/acs.jpca.7b00544
J. Phys. Chem. A 2017, 121, 2748−2759

whether CH_3O or CH_2OH is the neutral fragment. Though the former requires a direct bond breaking in the parent ion, which is associated with a loose transition state and suggests a competitive, fast dissociation, the latter product is more stable by about 400 meV, at a computed dissociation energy of 11.42 eV. Indeed, once the intermediate ion [**21**] at 10.87 eV is formed over a transition state of 11.78 eV, the CH_2OH group may leave without a reverse barrier. This explains the low-energy formation mechanism of CH_3OCO^+at m/z = 59, and it also makes it less likely that the system will perform a methyl transfer to yield $CH_3OHCH_2^+$ [**22**] and eventually $CH_3OCH_2^+$ [**24**] at m/z = 45. Therefore, the m/z = 45 channel is suggested to take place via the ethanol intermediate, and the added m/z = 59 abundance above the 11.9 eV photon energy is probably thanks to direct bond rupture in the parent ion.

3.4. Unimolecular Dissociation Model. The appearance of the DMC breakdown diagram together with dissociation energy and reaction path calculations establish a preliminary dissociative photoionization model. It can now be fitted to reproduce the measurement and derive experimental appearance energies (Figure 3).[55] The four main parallel decay channels of the parent ion are governed by two rate determining isomerization steps. At low energies, the channels leading to m/z = 31 and 62 open up, and the asymmetric daughter ion peak shape (Figure 2) below a photon energy of 11.45 eV indicates a metastable dissociation. The partitioning of the reactive flux into the CH_3 + CO_2-loss channel and the CO-loss channel probably takes place shortly after the first H-transfer isomerization step, and the threshold energy to dissociation is determined experimentally as $E_0(CH_2OH^+)$ = 11.14 ± 0.01 eV and $E_0(C_2H_6O_2^+)$ = 11.16 ± 0.05 eV. On the basis of the absence of a sequential water-loss signal from $C_2H_6O_2^+$ and its main dissociation product at m/z = 33, $CH_3OH_2^+$, we argue that m/z = 62 is predominantly ethylene glycol, although we could not find an energetically feasible path to form it from the parent ion. The breakdown curve for m/z = 33 could be reproduced faithfully at the onset of the fragment ion signal using statistical product energy distribution in the CO-loss step, which suggests that, in contrast to the m/z = 31 channel associated with a large kinetic energy release, the product energy distribution is statistical in the m/z = 62 channel. The fitted 0 K appearance energy for protonated methanol, $E_0(CH_3OH_2^+)$ = 11.54 ± 0.03 eV, only 0.38 eV above the m/z = 62 onset, indicates that the m/z = 62 intermediate sits in a shallow potential energy well.

In the high-energy range, two further parallel channels rise, namely, 45 amu loss and 31 amu loss leading to fragment ions at m/z = 45 and 59. The former corresponds to CO_2 leaving the parent ion and leaving behind a highly energetic intermediate ethanol cation that loses a hydrogen atom immediately. The second, the loss of CH_2OH or CH_3O yields CH_3OCO^+, and the former neutral fragment is associated with a lower barrier and a tighter transition state, whereas the latter neutral can be released in a simple C−O bond rupture. The fitted appearance energies for the two channels are 11.47 ± 0.06 and 11.46 ± 0.04 eV. Above 11.9 eV, the m/z = 59 abundance starts to rise more rapidly, thanks to the opening up of the fast but higher-energy direct bond rupture process. In the same energy range, the model starts underestimating the fractional abundance of CH_2OH^+ at m/z = 31 and overestimating that of m/z = 33. This is probably due to the fact that CH_2OH^+ is also a minor dissociation product of ethylene glycol cation, a channel unaccounted for in the statistical model and in competition with m/z = 33 formation. Furthermore, the fragmentation of the unseen intermediate ethanol cation at m/z = 46 may also contribute to the m/z = 31 signal by methyl loss at higher energies.[73]

3.5. Thermochemical Calculations. To anchor the measured appearance energies to the standard enthalpy of formation scale, we must address the enthalpy of formation of dimethyl carbonate. We set up two reactions, an isodesmic and an isomerization reaction, which connect DMC to species with better defined thermochemistry, namely methanol, formic acid, formaldehyde, water, and 1,3,5-trioxane, a six-membered ring trimer of formaldehyde:

$$2CH_3OH + 2HCOOH \rightarrow C_3H_6O_3\ (DMC) + H_2CO + 2H_2O \quad (2)$$

$$C_3H_6O_3\ (1,3,5\text{-trioxane}) \rightarrow C_3H_6O_3\ (DMC) \quad (3)$$

The gas-phase 0 K enthalpies of formation of the first four compounds are listed in the 1.118 version of the Active Thermochemical Tables[74−77] (ATcT) as −189.84 ± 0.17, −371.20 ± 0.24, −105.32 ± 0.11, and −238.93 ± 0.03 kJ mol^{-1}, respectively. Pedley lists the room temperature gas-phase heat of formation of trioxane as −465.90 ± 0.50 kJ mol^{-1},[78] which converts to −439.49 kJ mol^{-1} at 0 K using the average CBS-APNO, W1, and G4 computed thermal enthalpy of 15.17 kJ mol^{-1} and the elemental thermal enthalpies.[79] The calculated reaction energies for (2) are −12.16, −13.71, and −10.19, and for (3) −108.3, −107.4, and −107.7 kJ mol^{-1} using the G4, CBS-APNO, and W1U composite methods, respectively. On average, the derived enthalpy of formation for DMC is obtained as $\Delta_fH^\circ_{0K}(DMC(g))$ = −548.3 ± 1.5 kJ mol^{-1}, which converts to $\Delta_fH^\circ_{298K}(DMC(g))$ = −571.6 ± 1.5 kJ mol^{-1}. Using the measured ionization energy of 10.47 eV, the enthalpy of formation of the cation is thus obtained as $\Delta_fH^\circ_{0K}(DMC^+)$ = 461.9 ± 1.8 kJ mol^{-1} in the stationary electron convention. Furthermore, together with the appearance energy for CH_2OH^+, 11.14 ± 0.01 eV, i.e., 1074.8 kJ mol^{-1}, the heat of formation of the activated complex is obtained as $\Delta_fH^\circ_{0K}([\mathbf{5}]^\ddagger)$ = 526.5 kJ mol^{-1}. Based on the heats of formation of the DPI products, $\Delta_fH^\circ_{0K}(CO_2(g))$ = −393.11 ± 0.02 kJ mol^{-1}, $\Delta_fH^\circ_{0K}(CH_3)$ = 149.84 ± 0.08 kJ mol^{-1} from ATcT 1.118, and $\Delta_fH^\circ_{0K}(CH_2OH^+)$ = 717.7 ± 0.7 kJ mol^{-1},[80] in sum 474.4 kJ mol^{-1}, the overall reverse barrier to m/z = 31 formation in dissociative photoionization is determined as 52 kJ mol^{-1} or 0.54 eV, significantly above the computed value of 0.01 eV. This also explains the large kinetic energy release observed as the broadening of the parent ion peak in the 11.055 and 11.115 eV mass spectra.

Taking into account the room temperature vaporization enthalpy of DMC of Δ_f^gH = 38.02 ± 0.19 kJ mol^{-1},[81] the enthalpy of formation of liquid dimethyl carbonate is obtained as $\Delta_fH^\circ_{298K}(DMC(g))$ = −609.6 ± 1.5 kJ mol^{-1}. This can be used to derive the heat of combustion of DMC according to

$$C_3H_6O_3(l,DMC) + 3O_2(g) \rightarrow 3H_2O(l) + 3CO_2(g) \quad (4)$$

using $\Delta_fH^\circ_{298K}(CO_2(g))$ = −393.47 ± 0.02 kJ mol^{-1} and $\Delta_fH^\circ_{298K}(H_2O(l))$ = −285.83 ± 0.03 kJ mol^{-1}, as listed in ATcT 1.118. $\Delta_rH_{298K}(4)$ = 1428.3 ± 1.5 kJ mol^{-1} ≡ 15.87 ± 0.02 MJ kg^{-1}, which is slightly more than half of the analogously defined heat of combustion of ethanol per weight, Δ_rH_{298K} = 1367 kJ mol^{-1} ≡ 29.7 MJ kg^{-1} (also based on ATcT 1.118), resulting in lower combustion temperatures and

DOI: 10.1021/acs.jpca.7b00544
J. Phys. Chem. A 2017, 121, 2748−2759

suppressing NO_x formation in a similar combustion environment.

4. CONCLUSIONS

Threshold photoelectron photoion coincidence experiments were conducted on dimethyl carbonate in the 10.3−12.5 eV photon energy range. DMC formed a stable parent ion at the ionization onset, and the Franck−Condon analysis of the vibrational fine structure in the ground state band of the photoelectron spectrum helped identify the active C—O—C bending and C═O stretching modes upon ionization. The adiabatic ionization energy of DMC could also be determined as 10.47 eV. The breakdown diagram was analyzed to determine the dissociative photoionization mechanism, and *ab initio* calculations were carried out to explore the potential energy surface and locate the rate determining transition states. The DMC^+ cation dissociates by four parallel pathways: CH_3 + CO_2 loss yields the lightest fragment observed herein at m/z = 31, CH_2OH^+, at a 0 K appearance energy of 11.14 eV. In parallel, the parent ion may lose CO to yield what is suggested to be the ethylene glycol cation at m/z = 62 and an onset of 11.16 eV. However, the reaction pathway to ethylene glycol was not found on the potential energy surface. Two further parallel channels open up at higher energies, CO_2 + H loss yielding m/z = 45 over the ethanol intermediate and CH_2OH loss yielding $OCOCH_3^+$ at m/z = 59. The fitted appearance energies are 11.46 and 11.47 eV, respectively. At higher energies, CH_3O loss by C—O bond breaking contributes to the m/z = 59 channel, as well. The m/z = 62 fragment ion dissociates further to m/z = 33 at an onset of 11.54 eV. At higher energies, the m/z = 33 contribution is overestimated, the m/z = 31 is underestimated by the statistical model, which indicates a further, parallel dissociation channel from m/z = 62, yielding m/z = 31, which is not included in the model but is consistent with m/z = 62 being the ethylene glycol cation. A further contributor to the m/z = 31 signal may be the ethanol intermediate, which also decays by methyl radical loss at higher internal energies.

With the exception of the ethylene glycol path, the reaction coordinates could be identified satisfactorily on the potential energy surface of the DMC^+ cation. However, calculations suggest that numerous, energetically close lying minima and transition states play a role, whereas the breakdown diagram suggests that two rate-determining transition states govern the dissociation mechanism, one for the m/z = 31 and 62 channels, and another for the m/z = 45 and 59 channels. This apparent dichotomy may be resolved if the apparent simplicity of the breakdown diagram is the result of the superposition of complex reaction pathways. Nevertheless, the statistical DPI model can still be used to predict the threshold ionization mass spectrum of DMC below 12 eV at an arbitrary temperature, assisting, for instance, pyrolysis or combustion experiments.

At the same time, it is an unusual and intriguing observation that the first dissociation channel yields the lightest fragment ion of all in the studied energy range, which, at m/z = 31, dominates the breakdown diagram until it is overtaken by the m/z = 45 and then by the m/z = 59 signal. Thus, the more energy is available for the dissociation, the larger the fragment ions. Furthermore, several dissociation steps take place inevitably in multiple steps with intermediate ions barely (at m/z = 75 in CH_3 loss followed by CO_2 loss) or not at all observable (in CO_2 loss followed by H loss). Highly exothermic isomerization steps and stable leaving groups make such processes possible.

Finally, to relate the derived onset energies to the standard thermochemical scale, we calculated isodesmic and isomerization reaction energies to determine the heat of formation of DMC as $\Delta_f H^\circ_{298K}(DMC(g)) = -571.6 \pm 1.5$ kJ mol^{-1}. Overall, the combustion enthalpy of DMC is about half of that of ethanol per unit mass.

AUTHOR INFORMATION

Corresponding Authors

*X. Zhou. E-mail: xzhou@ustc.edu.cn.
*A. Bodi. E-mail: andras.boedi@psi.ch.

ORCID

Xiaoguo Zhou: 0000-0002-0264-0146
Andras Bodi: 0000-0003-2742-1051

Notes

The authors declare no competing financial interest.

ACKNOWLEDGMENTS

The experimental work was carried out at the VUV beamline of the Swiss Light Source of the Paul Scherrer Institute. The financial support of the Swiss Federal Office for Energy (BFE Contract No. SI/501269-01) and the National Natural Science Foundation of China (Nos. 21373194 and21573210) are gratefully acknowledged. X. Wu and X. Zhou also appreciate the support from the Chinese exchange student grant and the Ministry of Science and Technology of China (No. 2012YQ220113).

REFERENCES

(1) Memoli, S.; Selva, M.; Tundo, P. Dimethylcarbonate for Eco-Friendly Methylation Reactions. *Chemosphere* **2001**, *43*, 115−121.
(2) Ono, Y. Dimethyl Carbonate for Environmentally Benign Reactions. *Catal. Today* **1997**, *35*, 15−25.
(3) Tundo, P. New Developments in Dimethyl Carbonate Chemistry. *Pure Appl. Chem.* **2001**, *73*, 1117−1124.
(4) Tundo, P.; Selva, M. The Chemistry of Dimethyl Carbonate. *Acc. Chem. Res.* **2002**, *35*, 706−716.
(5) G.-A. Nazri, G. P. E. Lithium Batteries. *Science and Technology*; Kluwer Academic Publisher: Dordrecht, New York, London, 2004.
(6) Pacheco, M. A.; Marshall, C. L. Review of Dimethyl Carbonate (Dmc) Manufacture and Its Characteristics as a Fuel Additive. *Energy Fuels* **1997**, *11*, 2−29.
(7) Sun, W.; Yang, B.; Hansen, N.; Westbrook, C. K.; Zhang, F.; Wang, G.; Moshammer, K.; Law, C. K. An Experimental and Kinetic Modeling Study on Dimethyl Carbonate (Dmc) Pyrolysis and Combustion. *Combust. Flame* **2016**, *164*, 224−238.
(8) Katrib, Y.; Deiber, G.; Mirabel, P.; Le Calvé, S.; George, C.; Mellouki, A.; Le Bras, G. Atmospheric Loss Processes of Dimethyl and Diethyl Carbonate. *J. Atmos. Chem.* **2002**, *43*, 151−174.
(9) Huang, Z.; Jiang, D.; Zeng, K.; Liu, B.; Yang, Z. Combustion Characteristics and Heat Release Analysis of a Direct Injection Compression Ignition Engine Fuelled with Diesel—Dimethyl Carbonate Blends. *Proc. Inst. Mech. Eng., Part D* **2005**, *217*, 595−605.
(10) Bohets, H.; van der Vecken, B. J. On the Conformational Behavior of Dimethyl Carbonate. *Phys. Chem. Chem. Phys.* **1999**, *1*, 1817−1826.
(11) Kar, B. P.; Ramanathan, N.; Sundararajan, K.; Viswanathan, K. S. Conformations of Dimethyl Carbonate and Its Complexes with Water: A Matrix Isolation Infrared and Ab Initio Study. *J. Mol. Struct.* **2012**, *1024*, 84−93.
(12) Boussessi, R.; Guizani, S.; Senent, M. L.; Jaïdane, N. Theoretical Characterization of Dimethyl Carbonate at Low Temperatures. *J. Phys. Chem. A* **2015**, *119*, 4057−4064.
(13) Lovas, F. J.; Plusquellic, D. F.; Widicus Weaver, S. L.; McGuire, B. A.; Blake, G. A. Organic Compounds in the $C_3H_6O_3$ Family:

DOI: 10.1021/acs.jpca.7b00544
J. Phys. Chem. A 2017, 121, 2748−2759

Microwave Spectrum of Cis−Cis Dimethyl Carbonate. *J. Mol. Spectrosc.* **2010**, *264*, 10−18.
(14) Felsmann, D.; Moshammer, K.; Krüger, J.; Lackner, A.; Brockhinke, A.; Kasper, T.; Bierkandt, T.; Akyildiz, E.; Hansen, N.; Lucassen, A.; et al. Electron Ionization, Photoionization and Photoelectron/Photoion Coincidence Spectroscopy in Mass-Spectrometric Investigations of a Low-Pressure Ethylene/Oxygen Flame. *Proc. Combust. Inst.* **2015**, *35*, 779−786.
(15) Qi, F. Combustion Chemistry Probed by Synchrotron Vuv Photoionization Mass Spectrometry. *Proc. Combust. Inst.* **2013**, *34*, 33−63.
(16) Urness, K. N.; Guan, Q.; Golan, A.; Daily, J. W.; Nimlos, M. R.; Stanton, J. F.; Ahmed, M.; Ellison, G. B. Pyrolysis of Furan in a Microreactor. *J. Chem. Phys.* **2013**, *139*, 124305.
(17) Robichaud, D. J.; Nimlos, M. R.; Ellison, G. B. Pyrolysis Mechanisms of Lignin Model Compounds Using a Heated Micro-Reactor. In *Reaction Pathways and Mechanisms in Thermocatalytic Biomass Conversion I*; Springer: Singapore, 2016.
(18) Parker, D. S.N; Kaiser, R. I.; Troy, T. P.; Ahmed, M. Hydrogen Abstraction/Acetylene Addition Revealed. *Angew. Chem., Int. Ed.* **2014**, *53*, 7740−7744.
(19) Savee, J. D.; Papajak, E.; Rotavera, B.; Huang, H.; Eskola, A. J.; Welz, O.; Sheps, L.; Taatjes, C. A.; Zádor, J.; Osborn, D. L. Direct Observation and Kinetics of a Hydroperoxyalkyl Radical (QOOH). *Science* **2015**, *347*, 643−646.
(20) Baer, T.; Sztáray, B.; Kercher, J. P.; Lago, A. F.; Bödi, A.; Skull, C.; Palathinkal, D. Threshold Photoelectron Photoion Coincidence Studies of Parallel and Sequential Dissociation Reactions. *Phys. Chem. Chem. Phys.* **2005**, *7*, 1507−1513.
(21) Liang, S.; Hemberger, P.; Neisius, N. M.; Bodi, A.; Grützmacher, H.; Levalois-Grützmacher, J.; Gaan, S. Elucidating the Thermal Decomposition of Dimethyl Methylphosphonate by Vacuum Ultraviolet (VUV) Photoionization: Pathways to the PORadical, a Key Species in Flame-Retardant Mechanisms. *Chem. - Eur. J.* **2015**, *21*, 1073−1080.
(22) Bodi, A.; Hemberger, P.; Osborn, D. L.; Sztáray, B. l. Mass-Resolved Isomer-Selective Chemical Analysis with Imaging Photoelectron Photoion Coincidence Spectroscopy. *J. Phys. Chem. Lett.* **2013**, *4*, 2948−2952.
(23) Holzmeier, F.; Lang, M.; Hemberger, P.; Bodi, A.; Schäfer, M.; Dewhurst, R. D.; Braunschweig, H.; Fischer, I. Photoionization and Pyrolysis of a 1, 4-Azaborinine: Retro-Hydroboration in the Cation and Identification of Novel Organoboron Ring Systems. *Chem. - Eur. J.* **2014**, *20*, 9683−9692.
(24) Bouwman, J.; Bodi, A.; Oomens, J.; Hemberger, P. On the Formation of Cyclopentadiene in the C_3H_5·+ C_2H_2 Reaction. *Phys. Chem. Chem. Phys.* **2015**, *17*, 20508−20514.
(25) Voronova, K.; Mozaffari Easter, C. M.; Torma, K. G.; Bodi, A.; Hemberger, P.; Sztáray, B. Bifurcated Dissociative Photoionization Mechanism of Acetic Acid Anhydride Revealed by Imaging Photoelectron Photoion Coincidence Spectroscopy. *Phys. Chem. Chem. Phys.* **2016**, *18*, 25161−25168.
(26) Heringa, M. F.; Slowik, J. G.; Prévôt, A. S.H; Baltensperger, U.; Hemberger, P.; Bodi, A. Dissociative Ionization Mechanism and Appearance Energies in Adipic Acid Revealed by Imaging Photoelectron Photoion Coincidence, Selective Deuteration, and Calculations. *J. Phys. Chem. A* **2016**, *120*, 3397−3405.
(27) Linstrom, P. J.; Mallard, W. G.; Eds Nist Chemistry Webbook; Nist Standard Reference Database Number 69; National Institute of Standards and Technology: Gaithersburg, MD, http://webbook.nist.gov.
(28) Meeks, J. L.; Arnett, J. F.; Larson, D.; McGlynn, S. P. Photoelectron Spectroscopy of Carbonyls. Ionization Assignments. *Chem. Phys. Lett.* **1975**, *30*, 190−194.
(29) McGlynn, S. P.; Meeks, J. L. Photoelectron Spectra of Carbonyls, Carbonates, Oxalates and Esterification Effects. *J. Electron Spectrosc. Relat. Phenom.* **1976**, *8*, 85−93.
(30) Wittel, K.; Astrup, E. E.; Bock, H.; Graeffe, G.; Juslen, H. Photoelectron Spectra and Molecular Properties, Xlviii Carbonates and Thiocarbonates. *Z. Naturforsch., B: J. Chem. Sci.* **1975**, *30*, 862−874.
(31) Blanchette, M. C.; Holmes, J. L.; Hop, C. E. C. A.; Lossing, F. P.; Postma, R. J. A.; Ruttink, P.; Terlouw, J. Theory and Experiment in Concert: The [Meoc: O]+ Ion and Its Isomers. *J. Am. Chem. Soc.* **1986**, *108*, 7589−7594.
(32) Briggs, P. R.; Shannon, T. W. Heat of Formation of the Methoxycarbonyl Ion. *J. Am. Chem. Soc.* **1969**, *91*, 4307−4309.
(33) Wang, J.; Yang, B.; Cool, T. A.; Hansen, N. Absolute Cross-Sections for Dissociative Photoionization of Some Small Esters. *Int. J. Mass Spectrom.* **2010**, *292*, 14−22.
(34) Suh, D.; Kingsmill, C. A.; Ruttink, P. J.A.; Burgers, P. C.; Terlouw, J. K. C-H···O and O···H···O Bonded Intermediates in the Dissociation of Low Energy Methyl Glycolate Radical Cations. *Int. J. Mass Spectrom. Ion Processes* **1995**, *146*, 305−322.
(35) Fell, L. M.; Burgers, P. C.; Ruttink, P. J.A.; Terlouw, J. K. The Decarbonylation of Ionized B-Hydroxypyruvic Acid: The Hydrogen-Bridged Radical Cation $[CH2{=}O{\cdots}H{\cdots}O{=}C\text{-}OH]^{\cdot+}$ Studied by Experiment and Theory. *Can. J. Chem.* **1998**, *76*, 335−349.
(36) Fell, L. M.; Ruttink, P. J.; Burgers, P. C.; Trikoupis, M. A.; Terlouw, J. K. Dissociation Chemistry of the Hydrogen-Bridged Radical Cation $CH_2{=}O{\cdots}H{\cdots}O{=}C\text{-}OCH_3]^{\cdot+}$: Proton Transport Catalysis and Charge Transfer. *Int. J. Mass Spectrom.* **2000**, *195*, 85−99.
(37) Trikoupis, M. A.; Terlouw, J. K.; Burgers, P. C.; Peres, M.; Lifshitz, C. How Do Dimethyl Oxalate Ions $CH_3O\text{-}C(=O)\text{-}C(=O)\text{-}OCH_3^{\cdot+}$ Break in Half? Loss of $CH_3^{\cdot}$ + CO_2 Versus $CH_3O\text{-}C{=}O^{\cdot}$. *J. Am. Soc. Mass Spectrom.* **1999**, *10*, 869−877.
(38) Holmes, J. L.; Lossing, F. P.; Mayer, P. M. Heats of Formation of Oxygen-Containing Organic Free Radicals from Appearance Energy Measurements. *J. Am. Chem. Soc.* **1991**, *113*, 9723−9728.
(39) Bodi, A.; Baer, T.; Wells, N. K.; Fakhoury, D.; Klecyngier, D.; Kercher, J. P. Controlling Tunnelling in Methane Loss from Acetone Ions by Deuteration. *Phys. Chem. Chem. Phys.* **2015**, *17*, 28505−28509.
(40) Bodi, A.; Johnson, M.; Gerber, T.; Gengeliczki, Z.; Sztáray, B.; Baer, T. Imaging Photoelectron Photoion Coincidence Spectroscopy with Velocity Focusing Electron Optics. *Rev. Sci. Instrum.* **2009**, *80*, 034101.
(41) Hemberger, P.; Bodi, A.; Gerber, T.; Würtemberger, M.; Radius, U. Unimolecular Reaction Mechanism of an Imidazolin-2-Ylidene: An iPEPICO Study on the Complex Dissociation of an Arduengo-Type Carbene. *Chem. - Eur. J.* **2013**, *19*, 7090−7099.
(42) Hemberger, P.; Bodi, A.; Berthel, J. H.; Radius, U. Intramolecular C- N Bond Activation and Ring-Expansion Reactions of N-Heterocyclic Carbenes. *Chem. - Eur. J.* **2015**, *21*, 1434−1438.
(43) Muller, G.; Voronova, K.; Sztáray, B.; Meloni, G. Rotamers and Migration: Investigating the Dissociative Photoionization of Ethylenediamine. *J. Phys. Chem. A* **2016**, *120*, 3906−3916.
(44) Johnson, M.; Bodi, A.; Schulz, L.; Gerber, T. Vacuum Ultraviolet Beamline at the Swiss Light Source for Chemical Dynamics Studies. *Nucl. Instrum. Methods Phys. Res., Sect. A* **2009**, *610*, 597−603.
(45) Bodi, A.; Sztáray, B.; Baer, T.; Johnson, M.; Gerber, T. Data Acquisition Schemes for Continuous Two-Particle Time-of-Flight Coincidence Experiments. *Rev. Sci. Instrum.* **2007**, *78*, 084102.
(46) Sztáray, B.; Baer, T. Suppression of Hot Electrons in Threshold Photoelectron Photoion Coincidence Spectroscopy Using Velocity Focusing Optics. *Rev. Sci. Instrum.* **2003**, *74*, 3763−3768.
(47) Peng, C.; Ayala, P. Y.; Schlegel, H. B.; Frisch, M. J. Using Redundant Internal Coordinates to Optimize Equilibrium Geometries and Transition States. *J. Comput. Chem.* **1996**, *17*, 49−56.
(48) Curtiss, L. A.; Redfern, P. C.; Raghavachari, K. Gaussian-4 Theory. *J. Chem. Phys.* **2007**, *126*, 084108.
(49) Borkar, S.; Sztáray, B. Self-Consistent Heats of Formation for the Ethyl Cation, Ethyl Bromide, and Ethyl Iodide from Threshold Photoelectron Photoion Coincidence Spectroscopy. *J. Phys. Chem. A* **2010**, *114*, 6117−6123.
(50) Ochterski, J. W.; Petersson, G. A.; Montgomery, J. A., Jr A Complete Basis Set Model Chemistry. V. Extensions to Six or More Heavy Atoms. *J. Chem. Phys.* **1996**, *104*, 2598−2619.

DOI: 10.1021/acs.jpca.7b00544
J. Phys. Chem. A 2017, 121, 2748−2759

(51) Barnes, E. C.; Petersson, G. A.; Montgomery, J. A., Jr; Frisch, M. J.; Martin, J. M. Unrestricted Coupled Cluster and Brueckner Doubles Variations of W1 Theory. *J. Chem. Theory Comput.* **2009**, *5*, 2687−2693.
(52) Mozhayskiy, V.; Krylov, A. *ezSpectrum*; University of Southern California Los Angeles: Los Angeles, CA, 2008.
(53) Shao, Y.; Gan, Z.; Epifanovsky, E.; Gilbert, A. T.B.; Wormit, M.; Kussmann, J.; Lange, A. W.; Behn, A.; Deng, J.; Feng, X.; et al. Advances in Molecular Quantum Chemistry Contained in the Q-Chem 4 Program Package. *Mol. Phys.* **2015**, *113*, 184−215.
(54) Frisch, M. J; Trucks, G. W.; Schlegel, H. B.; Scuseria, G. E.; Robb, M. A.; Cheeseman, J. R.; Scalmani; Barone, V.; Mennucci, B.; Petersson, G. A.; et al. *Gaussian 09*; Gaussian, Inc.: Wallingford, CT, USA, 2009.
(55) Sztáray, B.; Bodi, A.; Baer, T. Modeling Unimolecular Reactions in Photoelectron Photoion Coincidence Experiments. *J. Mass Spectrom.* **2010**, *45*, 1233−1245.
(56) Marcus, R. A.; Rice, O. K. The Kinetics of the Recombination of Methyl Radicals and Iodine Atoms. *J. Phys. Chem.* **1951**, *55*, 894−908.
(57) Rice, O. K.; Ramsperger, H. C. Theories of Unimolecular Gas Reactions at Low Pressures. *J. Am. Chem. Soc.* **1927**, *49*, 1617−1629.
(58) Rice, O. K.; Ramsperger, H. C. Theories of Unimolecular Gas Reactions at Low Pressures. Ii. *J. Am. Chem. Soc.* **1928**, *50*, 617−620.
(59) Sztáray, B.; Baer, T. Consecutive and Parallel Dissociation of Energy-Selected $Co(CO)_3NO^+$ Ions. *J. Phys. Chem. A* **2002**, *106*, 8046−8053.
(60) Truong, S.; Yencha, A.; Juarez, A.; Cavanagh, S.; Bolognesi, P.; King, G. Threshold Photoelectron Spectroscopy of H_2O and D_2O over the Photon Energy Range 12−40eV. *Chem. Phys.* **2009**, *355*, 183−193.
(61) Yencha, A.; Cormack, A.; Donovan, R.; Hopkirk, A.; King, G. Threshold Photoelectron Spectroscopy of HCl and DCl. *Chem. Phys.* **1998**, *238*, 109−131.
(62) Bodi, A.; Hemberger, P. Imaging Breakdown Diagrams for Bromobutyne Isomers with Photoelectron−Photoion Coincidence. *Phys. Chem. Chem. Phys.* **2014**, *16*, 505−515.
(63) Borkar, S.; Ooka, L.; Bodi, A.; Gerber, T.; Sztáray, B. Dissociative Photoionization of Sulfur Chlorides and Oxochlorides: Thermochemistry and Bond Energies Based on Accurate Appearance Energies. *J. Phys. Chem. A* **2010**, *114*, 9115−9123.
(64) Savee, J. D.; Zádor, J.; Hemberger, P.; Sztáray, B.; Bodi, A.; Osborn, D. L. Threshold Photoelectron Spectrum of the Benzyl Radical. *Mol. Phys.* **2015**, *113*, 2217−2227.
(65) Harvey, J.; Tuckett, R. P.; Bodi, A. Shining New Light on The Multifaceted Dissociative Photoionisation Dynamics of CCl_4. *Phys. Chem. Chem. Phys.* **2014**, *16*, 20492−20499.
(66) Harvey, J.; Bodi, A.; Tuckett, R. P.; Sztáray, B. Dissociation Dynamics of Fluorinated Ethene Cations: From Time Bombs ona Molecular Level to Double-Regime Dissociators. *Phys. Chem. Chem. Phys.* **2012**, *14*, 3935−3948.
(67) Bouwman, J.; Sztáray, B.; Oomens, J.; Hemberger, P.; Bodi, A. Dissociative Photoionization of Quinoline and Isoquinoline. *J. Phys. Chem. A* **2015**, *119*, 1127−1136.
(68) Bauer, C. A.; Grimme, S. How to Compute Electron Ionization Mass Spectra from First Principles. *J. Phys. Chem. A* **2016**, *120*, 3755−3766.
(69) Bhoorasingh, P. L.; West, R. H. Transition State Geometry Prediction Using Molecular Group Contributions. *Phys. Chem. Chem. Phys.* **2015**, *17*, 32173−32182.
(70) Zádor, J.; Miller, J. A. Adventures on the C_3H_5O Potential Energy Surface: OH^+Propyne, OH^+ Allene and Related Reactions. *Proc. Combust. Inst.* **2015**, *35*, 181−188.
(71) Burgers, P. C.; Holmes, J. L.; Hop, C. E.C.A.; Postma, R.; Ruttink, P. J.A.; Terlouw, J. K. The Isomeric $[C_2H_6O_2]^{\cdot+}$ Hydrogen-Bridged Radical Cations $[CH_2\text{-}O(H)...H\cdots O{=}CH_2]^{\cdot+}$,$[CH_3\text{-}O\cdots H\cdots O{=}CH_2]^{\cdot+}$, and $[CH_3\text{-}O(H)...H\cdots O{=}CH]^{\cdot+}$: Theory and Experiment. *J. Am. Chem. Soc.* **1987**, *109*, 7315−7321.
(72) Bodi, A.; Brannock, M. D.; Sztáray, B.; Baer, T. Tunneling in H Loss from Energy Selected Ethanol Ions. *Phys. Chem. Chem. Phys.* **2012**, *14*, 16047−16054.
(73) Bodi, A. Internal Energy Selection in Vacuum Ultraviolet Photoionization of Ethanol and Ethanol Dimers. *J. Chem. Phys.* **2013**, *139*, 144306.
(74) Ruscic, B.; Pinzon, R. E.; Morton, M. L.; von Laszevski, G.; Bittner, S. J.; Nijsure, S. G.; Amin, K. A.; Minkoff, M.; Wagner, A. F. Introduction to Active Thermochemical Tables: Several "Key" Enthalpies of Formation Revisited. *J. Phys. Chem. A* **2004**, *108*, 9979−9997.
(75) Ruscic, B.; Pinzon, R. E.; Von Laszewski, G.; Kodeboyina, D.; Burcat, A.; Leahy, D.; Montoy, D.; Wagner, A. F. Active Thermochemical Tables: Thermochemistry for the 21st Century. *J. Phys.: Conf. Ser.* **2005**, *16*, 561−570.
(76) Ruscic, B. Uncertainty Quantification in Thermochemistry, Benchmarking Electronic Structure Computations, and Active Thermochemical Tables. *Int. J. Quantum Chem.* **2014**, *114*, 1097−1101.
(77) Ruscic, B. *Active Thermochemical Tables* (ATcT) Values Based on Ver. 1.118 of the Thermochemical Network (2015), available at ATcT.anl.gov.
(78) Pedley, J. B. *Thermochemical Data and Structures of Organic Compounds*; TRC Data Series; Thermodynamics Research Center: College Station, TX, 1994.
(79) Chase, M. W. *NIST—JANAF Thermochemical Tables (Journal of Physical and Chemical Reference Data Monograph No. 9)*; American Institute of Physics: Washington, DC, 1998.
(80) Borkar, S.; Sztáray, B.; Bodi, A. Dissociative Photoionization Mechanism of Methanol Isotopologues (CH_3OH, CD_3OH, CH_3OD and CD_3OD) by Ipepico: Energetics, Statistical and Non-Statistical Kinetics and Isotope Effects. *Phys. Chem. Chem. Phys.* **2011**, *13*, 13009−13020.
(81) Kozlova, S. A.; Emel'yanenko, V. N.; Georgieva, M.; Verevkin, S. P.; Chernyak, Y.; Schäffner, B.; Börner, A. Vapour Pressure and Enthalpy of Vaporization of Aliphatic Dialkyl Carbonates. *J. Chem. Thermodyn.* **2008**, *40*, 1136−1140.

DOI: 10.1021/acs.jpca.7b00544
J. Phys. Chem. A 2017, 121, 2748−2759